Coherent Amplification of Continuous Laser Field via Superfluorescence

K. Kitano[*] and H. Maeda

Department of Physical Sciences, Aoyama Gakuin University, Kanagawa 252-5258, Japan

Superfluorescence (SF) is collective spontaneous emission wherein radiators spontaneously synchronize, resulting in an intense single-pulse emission. The avalanche radiation of photons is initiated by the first photon emitted into the SF propagation mode. Because this process is stochastic, the absolute phase of the SF changes randomly from shot to shot. We demonstrate that this phase can be controlled by seeding the SF with a resonant continuous-wave (CW) laser. The seed light was weak enough not to cause the stimulated emission but strong enough to inject the first photon into the SF propagation mode prior to injection by the radiators themselves. Cross-correlation measurements between the seeded SF and CW laser revealed that the seed light was coherently amplified by the SF. The amplification factor for the instantaneous intensity was estimated to be 7 orders of magnitude. These results will pave the way for the development of new types of quantum optical amplifiers.

Superfluorescence (SF) is a synchronous phenomenon that occurs in quantum mechanics. In the spontaneous emission process of isolated systems, radiators (such as atoms) relax from their excited states to ground states independently, emitting a radiation field whose intensity decays exponentially with time. In contrast, under the conditions of a relatively large density of radiators with a long coherence time, the transition dipole of each radiator can spontaneously synchronize to oscillate in phase, resulting in the emission of an intense single pulse, referred to as SF. The theory of SF was proposed by Dicke in 1954 [1] and first demonstrated in the 1970s [2]. Already, SF has been observed in various physical systems and is recognized as a fundamental phenomenon in quantum optics [3–9].

From the perspective of radiation fields, SF is a photon avalanche phenomenon triggered by the first photon emitted into the SF propagation mode. Furthermore, when the first photon is externally provided, SF can be considered a light-amplification process. In this direction of research, studies have been conducted to drive SF coherently by externally irradiating seed light [10–12]. Vrehen *et al.* used another SF as a seed light and experimentally derived the tipping angle of a system, which corresponds to the initial pulse area of SF [11]. They estimated that the peak intensity of seed light was amplified by approximately 7 orders of magnitude. However, their study did not discuss whether or not the amplification process was coherent. Mesyats *et al.* used an ultrashort microwave pulse to seed an emission based on the Cherenkov superradiance (SR) of extended electron bunches [12]. They demonstrated that the phase of seed light was successfully transferred to the SR. However, the amplification factor was estimated to be at most 40 dB (4 orders of magnitude) in power, owing to the noise emitted by electron density fluctuations and bunch edges.

In this Letter, we investigated SF fields emitted from rubidium (Rb) atomic vapor in a cell. By applying a continuous-wave (CW) laser as the seed light, we successfully estimated the performance of SF as an optical amplifier. Cross-correlation measurements between the seeded SF and CW laser revealed that the seed light was coherently amplified by the SF. The estimated amplification factor was 7 orders of magnitude.

The experimental arrangement is further described in the Supplemental Material [13]. In brief, we employed a 1 kHz Ti:sapphire laser system that produces 0.4 mJ, 100 fs laser pulses with a central wavelength of 840 nm. The output beam was split into two beams with variable delays. One beam, containing 80% of the total power, was used to generate 420 nm second harmonics applied as a pump pulse. The other pulse was used as the probe pulse for the sum frequency generation (SFG) spectroscopy. A pump beam was focused near the exit of a heated cylindrical glass cell containing Rb vapor. The Rb atoms were excited from the $5S$ ground state to the $6P$ state, and three subsequent emissions were detected: upper cascaded SF (UCSF), lower cascaded SF (LCSF), and yoked SF (YSF) [see Fig. 1(a)]. A distributed feedback laser (DFBL) with a maximum power of 3.5 mW was used, and the beam was split into two beams with variable delays. One beam, containing 10% of the power, was used as the seed light of the LCSF. The remaining 90% was used as the reference light in the cross-correlation measurements. The seed light was irradiated coaxially with the pump beam and focused 20 mm behind the focus of the pump beam.

The first feature of the SF fields shown in Fig. 1(a) appears in its polarization [14,15]. When the pump field is linearly polarized, the UCSF field is also linearly polarized in the same direction. In contrast, the LCSF and YSF fields
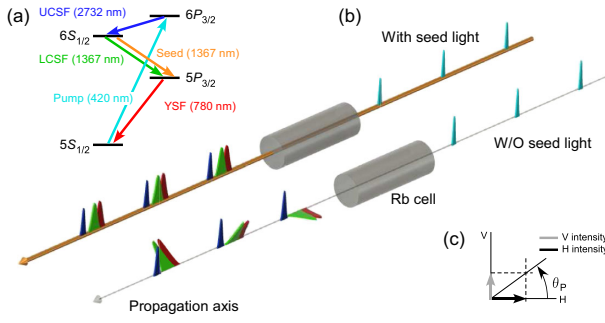
FIG. 1. (a) Energy diagram of Rb atoms and related transitions. (b) Schematic of three emission fields with and without seed light irradiation. (c) Definition of polarization angle.

are linearly polarized in the same direction with each other, but the direction changes randomly from shot to shot [14]. By actively exploiting the random nature of the polarization of LCSF, it is possible to distinguish whether the LCSF is triggered by an internal photon emitted from the atomic ensemble or by an external photon from the seed light. In the former case, the polarization directions of the LCSF and YSF are random. In the latter case, the direction is the same as that of the seed light [see Fig. 1(b)]. In the experiments, the field intensities of the vertical and horizontal polarizations were measured. The intensities were then used to define the polarization angle as shown in Fig. 1(c). Figure 2(a) shows the experimental results in the absence of seed light irradiation. In this figure, the polarization angles of LCSF and YSF are plotted as a function of the laser shot. They are almost synchronized and vary randomly for each laser shot. In Fig. 2(e), the data are plotted as a histogram, where the polarization angles are distributed uniformly between 0 and $\pi/2$ for both the LCSF and YSF. Figures 2(b)–2(d) and 2(f)–2(h) show the experimental results when the seed light is irradiated at a different power. The seed light is linearly polarized, and its polarization direction corresponds to $\theta_P = \pi/2$. Regarding the experimental results when the seed light power is 50 nW, for some shots, the LCSF is initiated by the photons of the seed light. This is evident by comparing Figs. 2(e) and 2(f). As the power increases, the probability increases where a photon of the seed light triggers the LCSF. Consequently, the polarization angles of LCSF and YSF become sharply distributed at approximately $\pi/2$. The above analysis predicts that the rise time of LCSF will be faster with an increase in seed power. To prove this, we conducted experiments to observe the temporal profiles of all three emissions by applying SFG spectroscopy [16].

The second feature of the SF fields shown in Fig. 1(a) appears in the relative time delays between the three emissions. The UCSF and LCSF are temporally separated because they are emitted by cascading transitions [17–19], $6P_{3/2} \to 6S_{1/2} \to 5P_{3/2}$. In contrast, the LCSF and YSF temporally overlap because the YSF is emitted by the nonlinear polarization [14,20–25] between the $5P_{3/2}$ and
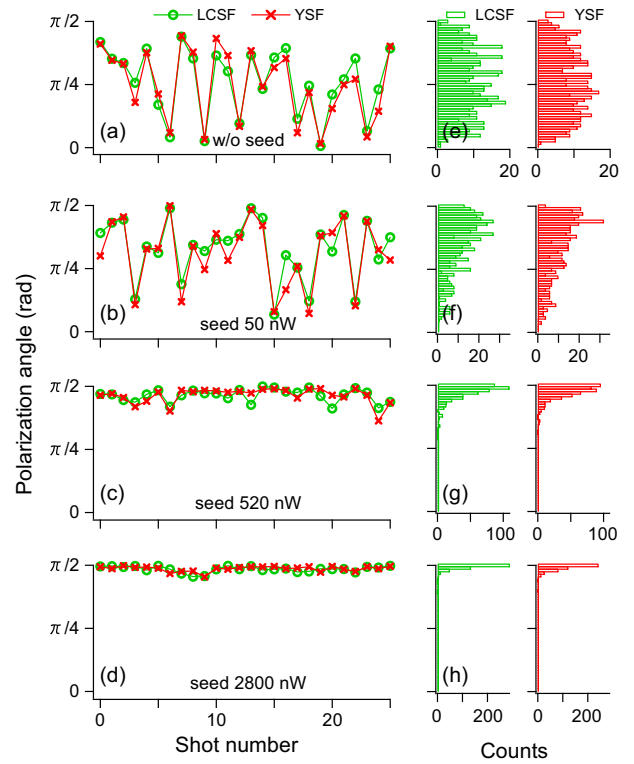

FIG. 2. (a) Measured polarization angles of the LCSF without the seed light irradiation plotted as a function of the shot number. (b)–(d) Same as (a), except the seed light is irradiated. (e)–(h) Distributions of polarization angles shown in (a)–(d), respectively, plotted as histograms.

$5S_{1/2}$ states created by the LCSF. Figures 3(a)–3(c) present the SFG signals of three emissions measured without the seed light, and with 520 and 1350 nW seed light, respectively, plotted as a function of the pump-probe delay. To compare the relative signal intensities, the vertical axes in Figs. 3(a)–3(c) are the same for each of the three emissions. Furthermore, because the SFG signal depends on the polarization of the SF field, the SFG signal intensity is calibrated based on the results of polarization experiments. The relative time delays between UCSF, LCSF, and YSF were consistent with those predicted above. Moreover, the rise times of the LCSF and YSF became faster as the power of the seed light increased. In contrast, the rise time of the UCSF remained unchanged. To validate these experimental results, we performed simulations by numerically solving the Maxwell-Bloch equations [16]. For the UCSF and LCSF, we introduced a constant Rabi frequency $\mu\varepsilon/\hbar$ as a boundary condition, where μ, ε, and $\hbar$ were the transition dipole moment, electric field envelope, and Planck's constant, respectively. The Rabi frequency is used because it is the Rabi frequency, not the electric field itself, that determines the dynamics associated with excitation and deexcitation of atoms when a constant ac electric field is applied to atoms in an isolated system. Without the seed light, the electric field envelope can be calculated by

$\varepsilon = \sqrt{n_e \hbar \omega \Omega_{so} L / T_{sp} c \varepsilon_0}$ [21], where ω, Ω_{so}, L, T_{sp}, n_e, c, and ϵ_0 are the angular frequency, solid angle of the SF emission, sample length, lifetime of an isolated atom, atomic number density in the excited state, speed of light, and vacuum permittivity, respectively. Note that the sample length is not the cell length, but the length along the optical axis of the region from which SF is emitted. With the seed light, the ε was estimated from the measured power and beam size of the seed light [13]. The pump intensity and sample length were then employed to reproduce the experimental results. The simulation results are summarized in Figs. 3(d)–3(f) to compare with the experimental results in Figs. 3(a)–3(c), respectively. The simulation results corroborated many of the features observed in the experimental results. First, the rise times of the LCSF and YSF became faster as the seed power increased, but that of the UCSF remained unchanged. Second, the simulated results reproduced the delay of the YSF peak relative to the LCSF peak. In particular, as in Figs. 3(e) and 3(f), the peak position of the LCSF could be quantitatively reproduced under seed light irradiation, supporting that the Rabi frequency as well as the electric field of the seed light was correctly evaluated. However, several points were not reproduced by the simulation results. For the UCSF, the ringing predicted by the simulation results was not observed in the experimental results. Further, for the LCSF and YSF, the experimental and simulation results do not match with respect to the structure that appears after the main peak. From the simulation, we confirmed that the ringing of UCSF and the time profiles after the main peak of LCSF and YSF can be significantly changed via slight variation in the excitation conditions or sample length. Therefore, the discrepancies between experimental and simulation results might be due to spatial averaging. The pump intensity used in the simulation was 0.6 times smaller than that estimated from the measured values. This is reasonable when considering the attenuation of the pump pulse during propagation inside the cell [16]. The sample length considered in the simulation was 9.0 mm.

Figure 3(g) presents the experimental results for the temporal profile of the LCSF when the wavelength of the seed light was swept. The horizontal and vertical axes correspond to the pump-probe delay and the seed wavelength, respectively. The power was fixed at 1320 nW. The experimentally observed resonance wavelength was 1366.88 nm, with an error of 0.02 nm from the actual resonance wavelength of 1366.900 nm. Throughout the study, the seed wavelength was fixed at 1366.88 nm.

The experimental results presented above demonstrate that the LCSF can be triggered by a photon of the seed light. To verify whether the LCSF was coherently driven by the seed light, we divided the DFBL into two parts: one was used as the seed light for the LCSF, and the other was used as the reference light. We then performed cross-correlation measurements between the LCSF and reference light.
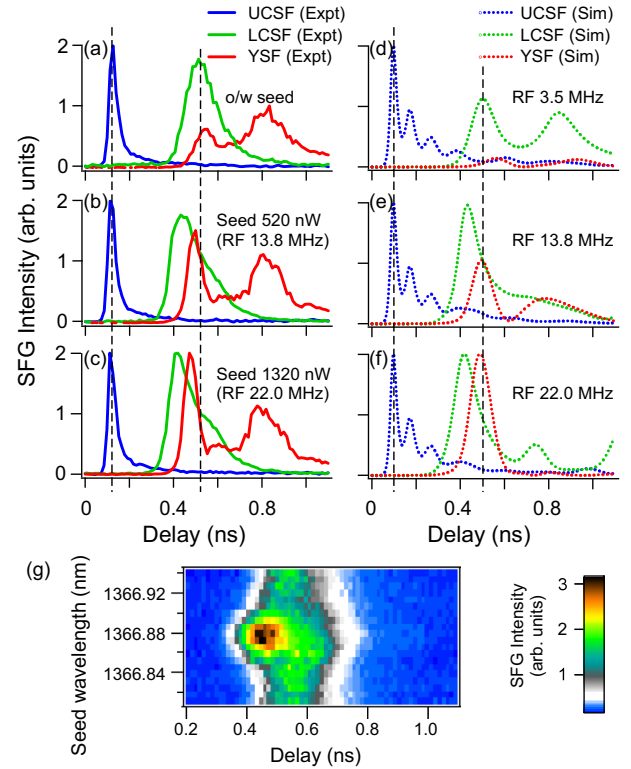

FIG. 3. (a) Temporal profiles of UCSF, LCSF, and YSF measured by SFG in the absence of seed light. (b),(c) Same as (a), except that the seed light is irradiated. The power of the seed light is shown in each figure. (d)–(f) Simulated temporal profiles of UCSF, LCSF, and YSF used to reproduce the results of (a)–(c), respectively. (g) Measured SFG signals of LCSF plotted against the pump-probe delay (horizontal axis) and the seed light wavelength (vertical axis).

Figure 4(a) shows the experimental results. The horizontal and vertical axes represent the oscilloscope time and the relative optical distance between the seed and reference light, respectively. As shown in Fig. 4(b), the LCSF appears as a peak around 2 ns on the oscilloscope. Notably, the reference light is continuous; therefore, it is observed as an offset voltage on the oscilloscope. When the seed light is blocked, a case that is denoted "Pump, Ref in" in Fig. 4(a), the LCSF intensity is constant and independent of the seed-reference delay. This is because there is no phase correlation between the nonseeded LCSF and reference light. When the seed light is irradiated, the LCSF intensity is periodically modulated with respect to the seed-reference delay. The power spectrum obtained after Fourier transforming the LCSF intensity is shown in Fig. 4(d), demonstrating that the modulation period coincides with the LCSF wavelength. These results demonstrate that the phase relationship between the seeded LCSF and reference light is well defined. Figure 4(c) depicts a cross-sectional view of Fig. 4(a) at the peak time of LCSF. Similar results were obtained for various seed-light powers. Next, we quantitatively evaluated the degree of coherence between the
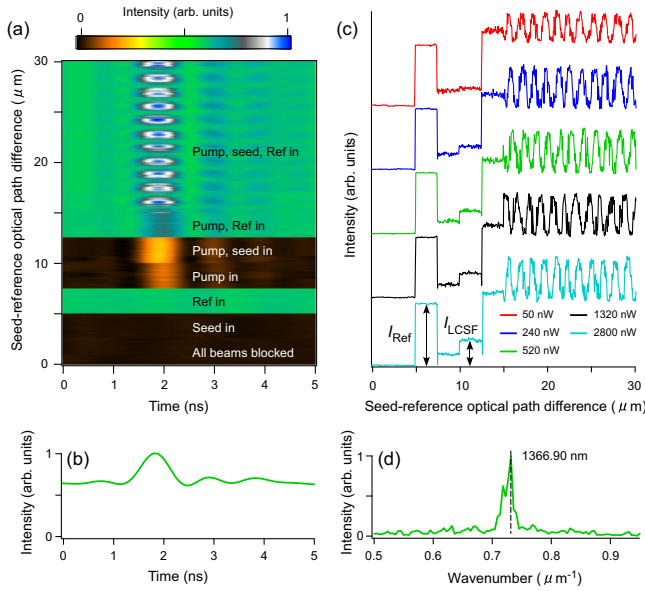
FIG. 4. (a) LCSF signal on oscilloscope plotted against oscilloscope time (horizontal axis) and seed-reference delay (vertical axis). (b) Typical oscilloscope signal. (c) Peak intensity of LCSF observed on the oscilloscope plotted against optical path difference. In the figure, the experimental results with various seed light powers are displayed. (d) Power spectrum obtained using the Fourier transform of the beat component of the experimental result in (c). The seed power was set to 520 nW.

seeded LCSF and reference light. As shown in Fig. 4(c), we denoted the intensity of the reference light and seeded LCSF as I_{Ref} and I_{LCSF}, respectively. The pulse width of LCSF in Fig. 4(b) is 3 times longer than that measured by SFG owing to the bandwidth limitation of the oscilloscope. Accordingly, the modulation signal can be calculated using the following equation:

$$I_{Mod} = \frac{2\sqrt{I_{Ref}(I_{LCSF}X_C)}}{\sqrt{3}}\cos\Delta\phi, \qquad (1)$$

where X_C and $\Delta\phi$ denote the fraction of the LCSF signal intensity that is coherent with the reference light and the relative phase between the two fields, respectively. The values of X_C estimated from the experimental results in Fig. 4(c) are 0.14, 0.25, 0.26, 0.25, and 0.23 for seed-light powers of 50, 240, 520, 1320, and 2800 nW, respectively. The X_C is almost unchanged above 240 nW of seed light, proving that 240 nW is sufficient to seed the LCSF. This result is consistent with the results of the polarization experiments shown in Fig. 2. There are two possible reasons why X_C was smaller than unity. The first is the possibility that the seeded LCSF and reference light were perfectly coherent with each other, but the amplitude of the modulation signal was reduced due to some problem associated with the measurement technique. Second, the seeded LCSF may contain a component that is incoherent

with the reference light. At this time, we believe that both possibilities cannot be ruled out.

It was demonstrated that LCSF is coherently driven by the seed light. More specifically, the instantaneous intensity of the seed light is coherently amplified by the SF. This indicates that the SF can serve as a coherent optical amplifier. The instantaneous intensities of seed light and SF are given by

$$I_{Seed} = P_{Seed}/A_{Seed},$$
$$I_{SF} = P_{SF}/(f_{Rep}\Delta T A_{SF}), \qquad (2)$$

where P_{Seed}, A_{Seed}, P_{SF}, A_{SF}, and ΔT are the seed light power, seed beam cross section, SF power, SF beam cross section, and pulse width of SF, respectively. We used the measured values of $P_{Seed} = 50$ nW, $P_{SF} = 100$ nW, and $\Delta T = 200$ ps. The f_{Rep} is a repetition rate of the pump pulse, which equals 1 kHz. As discussed in the Supplemental Material [13], the value of A_{Seed} and A_{SF} was estimated to be 8.3×10^{-4} and 7.5×10^{-5} cm^2, respectively. Substituting these values into Eq. (2) leads to $I_{SF}/I_{Seed} = 1.1 \times 10^8$, indicating that the instantaneous intensity of the seed light was amplified by 8 orders of magnitude via SF. Furthermore, by multiplying $X_C = 0.14$, the coherent amplification factor was calculated to be 1.5×10^7.

To validate this amplification factor, we provide a qualitative discussion of what determines it. Assuming that the spatial modes of seed light and SF are perfectly matched, the power required to seed the SF and the peak power of the SF are given by

$$P_{Seed} = \hbar\omega/T_R,$$
$$P_{SF} \approx n_e A_{SF} L\hbar\omega/T_R, \qquad (3)$$

respectively. The T_R is the collective radiation damping time defined as $T_R = T_{sp}8\pi/n_e\lambda^2 L$ [26], where λ is the wavelength of the emission field. From Eq. (3), the amplification factor is calculated to be $P_{SF}/P_{Seed} \approx n_e A_{SF} L = 8.1 \times 10^8$, which is 7 times larger than the experimentally obtained value of 1.1×10^8. As the values of A_{SF} and L are not the actual measured values for SF, this difference is considered to be within the error range.

In conclusion, we succeeded in coherently driving the LCSF via irradiation from a resonant seed light. Specifically, the instantaneous intensity of a seed light was coherently amplified by the LCSF by more than 7 orders of magnitude. It has been demonstrated that the superradiant laser can achieve spectral linewidths that cannot be realized with conventional lasers [27], proving the great potential of SF as an optical amplifier. However, it remains unclear how SF works as an amplifier, particularly for quantum light. Our method offers the unique physical system to investigate this, using one of entangled photon

pairs or a squeezed light as a seed light. For this purpose, it is necessary to achieve SF with sufficiently low photon flux [8,28–30].

———————————

[*]Corresponding author: kkitano@phys.aoyama.ac.jp

[1] R. H. Dicke, Coherence in spontaneous radiation processes, Phys. Rev. **93,** 99 (1954).

[2] N. Skribanowitz, I. Herman, J. MacGillivray, and M. Feld, Observation of Dicke superradiance in optically pumped HF gas, Phys. Rev. Lett. **30,** 309 (1973).

[3] P. Ding, M. Ruchkina, Z. Wang, M. Zhuzou, S. Xue, and J. Bood, Signature of femtosecond laser-induced superfluorescence from atomic hydrogen, Phys. Rev. A **105,** 013702 (2022).

[4] G. Findik, M. Biliroglu, D. Seyitliyev, J. Mendes, A. Barrette, H. Ardekani, L. Lei, Q. Dong, F. So, and K. Gundogdu, High-temperature superfluorescence in methyl ammonium lead iodide, Nat. Photonics **15,** 676 (2021).

[5] C. Braggio, F. Chiossi, G. Carugno, A. Ortolan, and G. Ruoso, Spontaneous formation of a macroscopically extended coherent state, Phys. Rev. Res. **2,** 033059 (2020).

[6] L. Mercadier, A. Benediktovitch, C. Weninger, M. A. Blessenohl, S. Bernitt, H. Bekker, S. Dobrodey, A. Sanchez-Gonzalez, B. Erk, C. Bomme *et al.*, Evidence of extreme ultraviolet superfluorescence in xenon, Phys. Rev. Lett. **123,** 023201 (2019).

[7] A. Angerer, K. Streltsov, T. Astner, S. Putz, H. Sumiya, S. Onoda, J. Isoya, W. J. Munro, K. Nemoto, J. Schmiedmayer *et al.*, Superradiant emission from colour centres in diamond, Nat. Phys. **14,** 1168 (2018).

[8] F. Jahnke, C. Gies, M. Aßmann, M. Bayer, H. Leymann, A. Foerster, J. Wiersig, C. Schneider, M. Kamp, and S. Höfling, Giant photon bunching, superradiant pulse emission and excitation trapping in quantum-dot nanolasers, Nat. Commun. **7,** 11540 (2016).

[9] H. M. Gibbs, Q. H. F. Vrehen, and H. M. J. Hikspoors, Single-pulse superfluorescence in cesium, Phys. Rev. Lett. **39,** 547 (1977).

[10] D. D. Grimes, S. L. Coy, T. J. Barnum, Y. Zhou, S. F. Yelin, and R. W. Field, Direct single-shot observation of millimeter-wave superradiance in Rydberg-Rydberg transitions, Phys. Rev. A **95,** 043818 (2017).

[11] Q. H. F. Vrehen and M. F. H. Schuurmans, Direct measurement of the effective initial tipping angle in superfluorescence, Phys. Rev. Lett. **42,** 224 (1979).

[12] G. A. Mesyats, N. S. Ginzburg, A. A. Golovanov, G. G. Denisov, I. V. Romanchenko, V. V. Rostov, K. A. Sharypov, V. G. Shpak, S. A. Shunailov, M. R. Ulmaskulov *et al.*, Phase-imposing initiation of Cherenkov superradiance emission by an ultrashort-seed microwave pulse, Phys. Rev. Lett. **118,** 264801 (2017).

[13] See Supplemental Material at http://link.aps.org/supplemental/10.1103/PhysRevLett.132.073201 for details

[14] K. Kitano, H. Tomida, D. Takei, and H. Maeda, Polarization correlation in the superfluorescent decay process, Opt. Lett. **46,** 5055 (2021).

[15] A. Crubellier, S. Liberman, and P. Pillet, Doppler-free superradiance experiments with Rb atoms: Polarization characteristics, Phys. Rev. Lett. **41,** 1237 (1978).

[16] K. Kitano and H. Maeda, Cascade and yoked superfluorescence detected by sum frequency generation spectroscopy, Opt. Lett. **48,** 69 (2023).

[17] F. Chiossi, C. Braggio, A. Khanbekyan, G. Carugno, A. Ortolan, G. Ruoso, R. Calabrese, A. Di Lieto, L. Tomassetti, and M. Tonelli, Cascade superfluorescence in Er: YLF, Phys. Rev. Res. **3,** 013138 (2021).

[18] J. Okada, K. Ikeda, and M. Matsuoka, Cooperative cascade emission, Opt. Commun. **26,** 189 (1978).

[19] M. Gross, C. Fabre, P. Pillet, and S. Haroche, Observation of near-infrared Dicke superradiance on cascading transitions in atomic sodium, Phys. Rev. Lett. **36,** 1035 (1976).

[20] J. H. Brownell, X. Lu, and S. R. Hartmann, Yoked superfluorescence, Phys. Rev. Lett. **75,** 3265 (1995).

[21] K. Kitano, M. Sato, Y. Komasaka, and H. Maeda, Nonlinear optical processes driven by superfluorescent fields and their controllability with external laser fields, Phys. Rev. A **102,** 031101(R) (2020).

[22] J. R. Harries, H. Iwayama, S. Kuma, M. Iizawa, N. Suzuki, Y. Azuma, I. Inoue, S. Owada, T. Togashi, K. Tono *et al.*, Superfluorescence, free-induction decay, and four-wave mixing: Propagation of free-electron laser pulses through a dense sample of helium ions, Phys. Rev. Lett. **121,** 263201 (2018).

[23] Z. Yi, P. K. Jha, L. Yuan, D. V. Voronine, G. O. Ariunbold, A. M. Sinyukov, Z. Di, V. A. Sautenkov, Y. V. Rostovtsev, and A. V. Sokolov, Observing the transition from yoked superfluorescence to superradiance, Opt. Commun. **351,** 45 (2015).

[24] G. O. Ariunbold, M. M. Kash, V. A. Sautenkov, H. Li, Y. V. Rostovtsev, G. R. Welch, and M. O. Scully, Observation of picosecond superfluorescent pulses in rubidium atomic vapor pumped by 100-fs laser pulses, Phys. Rev. A **82,** 043421 (2010).

[25] A. I. Lvovsky, S. R. Hartmann, and F. Moshary, Omnidirectional superfluorescence, Phys. Rev. Lett. **82,** 4420 (1999).

[26] M. Feld and J. MacGillivray, *Coherent Nonlinear Optics, Superradiance* (Springer-Verlag, Berlin, 1980).

[27] J. G. Bohnet, Z. Chen, J. M. Weiner, D. Meiser, M. J. Holland, and J. K. Thompson, A steady-state superradiant laser with less than one intracavity photon, Nature (London) **484,** 78 (2012).

[28] G. Ferioli, A. Glicenstein, F. Robicheaux, R. T. Sutherland, A. Browaeys, and I. Ferrier-Barbut, Laser-driven superradiant ensembles of two-level atoms near Dicke regime, Phys. Rev. Lett. **127,** 243602 (2021).

[29] J. Kim, D. Yang, S.-h. Oh, and K. An, Coherent single-atom superradiance, Science **359,** 662 (2018).

[30] W. Guerin, M. O. Araújo, and R. Kaiser, Subradiance in a large cloud of cold atoms, Phys. Rev. Lett. **116,** 083601 (2016).